optica

Kagome-fiber-based pulse compression of mid-infrared picosecond pulses from a Ho:YLF amplifier

K. Murari,[1,2,*] G. J. Stein,[4] H. Cankaya,[1,3] B. Debord,[5] F. Gérôme,[5] G. Cirmi,[1,3] O. D. Mücke,[1,3] P. Li,[1] A. Ruehl,[1] I. Hartl,[1] K.-H. Hong,[4] F. Benabid,[5] and F. X. Kärtner[1,2,3,4]

[1]Center for Free Electron Laser Science (CFEL), Deutsches Elektronen-Synchrotron (DESY) & Department of Physics, University of Hamburg, Notkestrasse 85, 22607 Hamburg, Germany
[2]Max-Planck Institute for Structure and Dynamics of Matter (MPSD), Luruper Chaussee 149, 22761 Hamburg, Germany
[3]The Hamburg Center for Ultrafast Imaging, Luruper Chaussee 149, 22761 Hamburg, Germany
[4]Department of Electrical Engineering and Computer Science and Research Laboratory of Electronics, Massachusetts Institute of Technology (MIT), Cambridge, Massachusetts 02139, USA
[5]GPPMM Group, Xlim Research Institute, UMR 7252 CNRS, University of Limoges, Limoges, France
*Corresponding author: Krishna.murari@desy.de

Received 20 April 2016; revised 23 June 2016; accepted 23 June 2016 (Doc. ID 262822); published 21 July 2016

Over the last decade, the development of ultrafast laser pulses in the mid-infrared (MIR) region has led to important breakthroughs in attosecond science and strong-field physics. However, as most such broadband MIR laser sources are near-IR pumped, the generation of high-intensity, long-wavelength MIR pulses is still a challenge, especially starting from picosecond pulses. Here we report, both experimentally and numerically, nonlinear pulse compression of sub-millijoule picosecond pulses down to sub-300 fs at 2050 nm wavelength in gas-filled Kagome-type hollow-core photonic crystal fibers for driving MIR optical parametric amplifiers. The pump laser is comprised of a compact fiber laser-seeded 2 μm chirped pulse amplification system based on a Ho:YLF crystal at 1 kHz repetition rate. Spectral broadening is studied for different experimental conditions with variations of gas pressure and incident pulse energies. The spectrally broadened 1.8 ps pulses with a Fourier-limited duration of 250 fs are compressed using an external prism-based compressor down to 285 fs and output energy of 125 μJ.

OCIS codes: (140.0140) Lasers and laser optics; (140.3280) Laser amplifiers; (140.3580) Lasers, solid-state.

http://dx.doi.org/10.1364/OPTICA.3.000816

1. INTRODUCTION

In recent years, high-energy, ultrashort mid-infrared (MIR) laser sources have experienced rapid technological advancements due to their wide range of application. Several important molecules offer resonances at the MIR wavelength, making them an optimum choice for spectroscopy [1]. Moreover, carrier-envelope phase (CEP)-stabilized few-cycle (sub-100 fs) laser pulses at long wavelengths are in high demand for complex experiments in attoscience and strong-field physics. For example, high-energy ultrashort long-wavelength pulses permit the study of novel regimes in photoionization of gases [2,3], including the breakdown of the dipole approximation [4] and the wavelength dependence of recollision physics [5,6], and the investigation of non-perturbative strong-field effects in solids such as the dynamical Franz–Keldysh effect [7,8] and high-order harmonic generation (HHG) from Bloch oscillations [9,10]. MIR optical parametric amplifiers (OPAs), pumped by sub-ps mJ-level 2 μm sources [11], optionally followed by filamentation and pulse self-compression in dielectrics [12,13], provide a direct path to such experiments. Moreover, when properly scaled in pulse energy to the multi-mJ level, IR pulses even permit the realization of bright coherent tabletop HHG sources in the water-window and keV x-ray region [14].

High-energy ultrashort pulses are generated using a combination of methods that rely on chirped pulse amplification (CPA), followed by nonlinear pulse-compression techniques. The state-of-the-art approach to generate these pulses uses frequency conversion and amplification via OPA. High-energy pump and seed for OPA eventually relies on CPA schemes followed by nonlinear spectral broadening [15,16]. However, access to the long MIR wavelengths has been limited due to the nearly exclusive use of near-infrared (NIR) pump sources at 800 nm and 1 μm [17]. Moreover, accessing long MIR wavelengths (>5 μm) requires OPAs based on non-oxide crystals, as most oxide crystals are either not transparent above 4–5 μm or have very low conversion efficiency [18] with a NIR pump. Development of non-oxide crystals like zinc germanium phosphide (2–8 μm) and optically patterned gallium arsenide (OP-GaAs, 2–12 μm), which require pumping at 2 μm, are very significant for MIR pulse generation due to better phase matching and higher conversion efficiency [19–21]. Hence, pumping of non-oxide nonlinear crystals with 2 μm laser sources with mJ-level energy and sub-ps pulses

Corrected 21 July 2016

are preferred for generating stable and coherent white-light continua as seed for MIR OPAs featuring self-CEP stabilization of the idler [22,23]. Recently, MIR OPA pumped from a holmium laser has been demonstrated [11,24]. However, due to the long pulse duration, seed source was derived from either difference frequency generation or from OPA at 1 μm, which adds extra complexity.

Nonlinear pulse compression in a waveguide is the most common approach for generation of femtosecond pulse durations and can be implemented in various ways—for instance, spectral broadening in noble gas-filled large-core hollow capillaries where the noble gas acts as a nonlinear medium. But due to their large core size, very high peak powers are required to achieve SPM-induced spectral broadening, and reducing the core size in turn limits the throughput efficiency. Gas-filled hollow-core photonic crystal fibers (HC-PCFs) offer significant downscaling of the core size and show low transmission loss with broad transmission bandwidth. HC-PCFs are mainly based on either photonic bandgap (PBG) or inhibited coupling (IC) [25]. HC-PCFs exhibit a large optical overlap with the silica core-surround, which limits its pulse energy handling to a few tens of micro-joules. In the last decade, major developments in HC-PCF have been achieved [26]. We have especially seen the emergence of a new light-guidance mechanism, namely IC. In IC-guiding HC-PCF—unlike PBG-guiding, whereby the core guided optical modes are prevented from coupling to the cladding via absence of cladding modes at the frequencies and effective indices of the core modes (i.e., existence of photonic bandgap)—the non-coupling of core-guided light with the cladding relies on a strong reduction of the optical field overlap between the modes residing in the core and those residing in the cladding. Such a coupling inhibition results from a stronger transverse mismatch between the core modes and cladding modes and a tighter confinement of the silica cladding modes within the silica web structure. As a result, this fiber can offer enlarged core diameter, low dispersion, and broad transmission bandwidth [27,28]. IC-based HC-PCFs are of advantage over both hollow capillaries and PBG-based fibers, guiding light over a large bandwidth and overcoming the damage threshold of solid-core fibers. These fibers have allowed for a dramatic reduction in transmission loss and have broken records in pulse-energy handling and compression [29,30], leading to the demonstration of 1 mJ 600 fs Yb laser beam handling [30]. Furthermore, these fibers, filled with gases apart from SPM, can also support a variety of nonlinear optical interactions including third-harmonic generation [31] and extreme nonlinear phenomena like high-harmonic generation [32,33].

The spectral-broadening phenomena in solid-core fibers can be broadly categorized into two different regimes: femtosecond (FR) and picosecond (PR). Although SPM plays a significant role in both these regimes, fundamentally different higher-order effects become significant depending on the pump pulse and fiber parameters. In FR, when pumping in normal GVD, spectral broadening is dominated by SPM while, in anomalous GVD, soliton fission and Raman interactions dominate. However, in PR, spectral broadening cannot be solely explained in terms of SPM and soliton fission, although in normal GVD SPM still dominates. In the case of anomalous GVD, as the input pulse duration increases, a phenomenon called modulation instability (MI) and the four-wave mixing process play significant roles in the initial dynamics of pulse propagation in the fiber, where the fast modulation on the pump pulse in the time domain can subsequently lead to breakup of the pulses, leading to a train of fs soliton-like pulses. It has also been shown that Raman soliton self-frequency shifting and dispersive-wave generation are also present and it can be said that the soliton-related dynamics in the anomalous GVD range are similar in both FR and PR. A detailed discussion of the fundamental differences in the different regimes is beyond the scope of this paper, but an elaborate review can be found in Ref. [34].

Most of the pulse-compression experiments demonstrated so far in Kagome fibers have used input pulses of sub-ps duration [15,35–37]. Consequently, due to the high peak power, the throughput pulse energy of those experiments was limited to few hundreds of micro-joule energy in the presence of air [30]. Recently, self-compression of 80 fs pulses down to the single-cycle regime in these fibers has been demonstrated [36]. However, transferring such a compression technique and ratio starting from energetic ps-longer pulses is still a pressing challenge. This is particularly true in the case of 2 μm laser systems for which fs pulse generation is still under development. However, due to the low dispersion of these fibers (typically 1 ps/nm/km), ps pulses experience hundreds of km-long dispersion lengths in these fibers, making self-compression impractical. Hence, pulse compression with these fibers for ps-long pulses can be realized in two steps: spectral broadening in the fiber and external compression to compensate for the chirp acquired.

Here, we demonstrate spectral broadening of 2.05 μm wavelength, 1.8 ps pulses from a Ho:YLF chirped-pulse amplifier system in air- and gas-filled Kagome fibers at a throughput energy of up to 700 μJ at 1 kHz and external pulse compression to 550 fs. We use two different fibers, a 7-cell and 19-cell core design with core diameters of 63 and 82 μm, respectively, at different input conditions for spectral broadening. The best compression is achieved with a 7-cell fiber at 238 μJ incident energy and Ar gas pressure of 5 bar. Finally, 1.8 ps pulses are compressed to 285 fs with Fourier-limited (FL) duration of 250 fs and more than 70% of the energy in the central peak. This is for the first time (to the best of our knowledge) compression of 2 μm ps laser pulses. We further study numerically the propagation of ps pulses in these fibers and the model matches the experimental behavior of spectral evolution for different input conditions.

2. EXPERIMENTAL DETAILS

A. Nonlinear Compression Setup

The laser system consists of a home-built Ho-doped fiber master oscillator and a prototype Ho:YLF regenerative amplifier (RA) followed by a single-pass booster amplifier (SPA) (Q-peak Inc.). Chirped Volume Bragg Gratings (CVBGs) are employed to stretch and compress the pulses due to their compactness and robustness against external disturbances. The RA cavity consists of a 0.5% doped 40 mm long Ho:YLF crystal, which is end-pumped by a continuous wave (CW) commercial Tm:fiber laser at 1938 nm, delivering up to ~50 W of random polarization. A frequency-selective linear filter, etalon of thickness 250 μm and reflectivity of 3.3%, is placed in the regen cavity to counteract the effect of gain narrowing in the amplifier. This technique enhances the effective gain bandwidth, thereby broadening the spectrum from 2.9 to 5.4 nm [38]. The RA output is subsequently amplified in an SPA, and the pulses are then compressed using a second identical CVBG. The net output of the amplifier (RA + SPA)

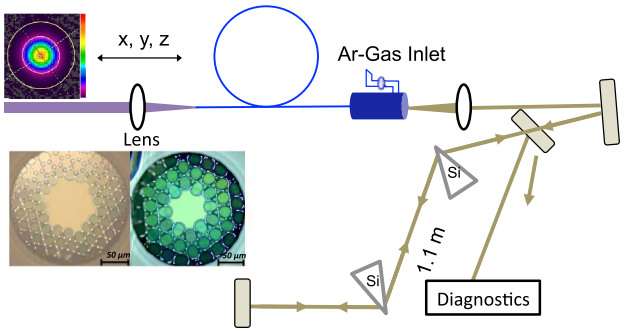

Fig. 1. Experimental setup for nonlinear pulse compression.

with a total pump power of 26 W pump power, is 2 mJ and 2.4 ps pulse duration. The output beam profile is characterized using a pyroelectric camera (Pyrocam III, Ophir-Spiricon Inc.) and exhibits a Gaussian profile. Complete details of the laser system can be found in [38].

The experimental setup of the nonlinear pulse compression is shown in Fig. 1. The linearly polarized output of the CPA system just explained is operated at lower pump power, to emit pulses of 1 mJ and 1.8 ps duration. These pulses are coupled through a focusing lens into the Kagome fiber. To investigate the transmission performance of the fiber, different coupling configurations were recorded. The beam diameter before the focusing lens is ~3 mm and three different lenses of focal length $f = 50$, 60, and 75 mm have been tested to optimize mode matching and maximize the transmission efficiency in the fiber. The input end of the fiber is mounted on a metal V-groove. To adjust the input coupling energy, a thin-film polarizer and a half-waveplate are used as a variable attenuator. The experiments are performed both in the presence of air and Ar gas pressure of 3 and 5 bar in 19-cell and 7-cell fiber.

B. Kagome-Type HC-PCF Fibers

Two different types of IC-guided Kagome HC-PCF fibers are used, with 7-cell and 19-cell cores based on a hypocycloid-core-contour designed for 2 μm wavelength operation and fabricated using the stack and draw technique. This new type of HC-PCF fiber offers relatively large core and low propagation losses. The physical and optical properties of both fibers are summarized in Fig. 2. The 19-cell fiber exhibits a hypocycloid core-contour of an inner core diameter of 82 μm corresponding to a mode-field diameter (MFD) of 58 μm. The 7-cell fiber has an inner core diameter of 63 μm, corresponding to a MFD of 44 μm. The outer diameters of the 19-cell and 7-cell fibers are 330 and 350 μm, respectively, whose numerical apertures are estimated to be 0.014 and 0.018, respectively. Figure 2(a) shows

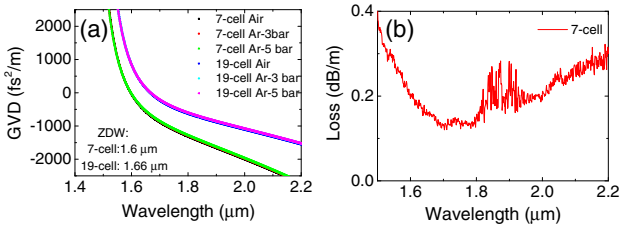

Fig. 2. (a) Calculated GVD of the 7-cell and 19-cell fibers. (b) Measured transmission loss versus wavelength of the 7-cell fiber.

the dispersion parameter as a function of wavelength simulated using a finite-element method for both 7-cell and 19-cell fibers under three different conditions: in air and in Ar gas pressure of 3 and 5 bar. Figure 2(b) shows the measured transmission loss along the extremely broad spectral range of 1400–2400 nm, exhibiting loss of 200 dB/km at 2050 nm. The unique transmission loss and bandwidth, in addition to the possibility of easily changing the gas as a nonlinear medium in the fiber to control the nonlinear coefficient, makes it an ideal choice for exploring high-energy ultrashort pulses. The broad transmission bandwidth of the Kagome fiber makes it unique among most of the known waveguides. The calculated GVD for both 7-cell and 19-cell fiber at the operating wavelength of 2050 nm is low and anomalous, with values of −2200 and −1200 fs^2/m, respectively.

3. RESULTS AND DISCUSSION

All the experiments shown subsequently are performed using a focusing lens, and the best coupling efficiency of 96% is achieved using the 50 mm focal length lens. It is noteworthy that the transmission efficiencies are also checked over several hours and several runs with the same fiber configuration, and no damage was observed. The output end of the fiber is capped in a high-pressure gas cell with a 5 mm thick uncoated CaF_2 window, while the input end is left open to the ambient air. As the input pulse duration is in the ps range, the output spectrum does not support very short pulse duration; hence GVD from the window is of very little significance and can be neglected. The first set of experiments is performed with 3.5 m of 19-cell fiber in the presence of ambient air. The experiments mostly rely on the fact that nonlinearity in these fibers can be easily tuned over the species of the gas present and its pressure. Most of the experiments published previously have demonstrated self-compression in these fibers in FR, which occurs due to interplay between the SPM and GVD. The SPM effect can be accounted for using the nonlinear length of the fiber, $L_{NL} = 1/\gamma P_0$, where $\gamma = 2\pi n_2/\lambda A_{eff}$ is the nonlinear parameter, n_2 is the nonlinear refractive index coefficient, and λ is the wavelength. The GVD effect is accounted for by the linear/dispersion length of the fiber given by $L_D = T_0^2/|\beta_2|$, where T_0 is the input pulse duration and β_2 is the negative GVD introduced in the fiber. Hence, we see that the dispersion length, which is proportional to the square of the input pulse duration, can be very long for ps pulses as compared to femtosecond pulses. Hence, self-compression of these ps-long pulses is not practical. Moreover, due to extremely long dispersion length, soliton order (N), which is defined as $N^2 = L_D/L_{NL}$, is very large ($N > 100$). This satisfies the condition of MI and makes the experiment prone toward any kind of fluctuations. Therefore, the spectrally broadened pulses are compressed using an external prism compressor whose apex separation is 1.1 m and a fixed prism insertion length of 10 mm. The distance is kept fixed throughout the experiments, which introduces a fixed negative second-order dispersion of ~150, 000 fs^2 and is optimized for the maximum broadened spectrum of ~88 nm, as will be further seen in the 7-cell experiments. Uncoated silicon Brewster-cut prisms of 1 inch height and an apex angle of 73.84° are used as the compressor. The second set of experiments is carried with the same fiber configuration but in the presence of argon (Ar) gas as a nonlinear medium at two different pressures of 3 and 5 bar. Similarly, the same experimental conditions were repeated with 7-cell Kagome fiber.

A. 19-Cell Kagome Fiber

Figure 3(a) shows the spectrum evolution of the pulse after propagating through a 3.5 m long 19-cell fiber (MFD = 58 μm) for different incident energies in the presence of ambient air. The fiber length was chosen to have enough nonlinearity in gas along the fiber but avoid the break-up of the pulse due to propagation of higher-order solitons. Figure 3(b) shows the measured autocorrelation traces (solid line) with the computed autocorrelation of the FL pulse corresponding to its respective spectrum (dashed lines). With increase in incident energy from 45 to 707 μJ, the spectral broadening scales linearly with energy. Without damaging the fiber, an incident energy as high as 707 μJ leads to foot-to-foot bandwidth of 77 nm, corresponding to a FL duration of 260 fs (FWHM). Thus, it leads to a maximum peak intensity of 3.5 and 17 TW/cm^2 at the input and output, respectively, and 5 times peak enhancement for the 19-cell fiber in presence of air. It can be seen in Fig. 3(b) that the shortest autocorrelation pulse duration is achieved with an input pulse energy of 707 μJ, resulting in an output pulse energy of 551 μJ, including the losses from the uncoated window of the gas cell.

Since it is known that nonlinear refractive index varies linearly with pressure at low pressures, we studied the effect of noble gas Ar on the spectral broadening at two different pressures of 3 and 5 bar. Ar has a high nonlinear refractive index coefficient $n_2 = 1.04 \times 10^{-19}$ cm^2/W at pressure of 1 bar and ionization potential of 15.76 eV. This leads to an n_2 value of 3.12×10^{-19} and 5.2×10^{-19} cm^2/W at 3 and 5 bar pressure, respectively [39]. (*It is to be noted that the n_2 value here corresponds to 800 nm and 50 fs pulse.*) Thus, Ar leads to a sufficiently high nonlinearity to produce spectral broadening with nonlinear length of 21 and 12 cm for 3 and 5 bar Ar pressure, respectively. $L_{NL} = (\gamma P_p)^{-1}$, where P_p is the peak power in the fiber core, and its ionization potential limits the incident energy to ~300 μJ. This is due to the fact that the type of gas used leads to photoionization and subsequent plasma absorption. Figure 4(a) summarizes the broadening obtained at different incident energy in 19-cell fiber in the presence of air and Ar pressure of 3 and 5 bar, while Fig. 4(b) summarizes the measured pulse duration for the corresponding energy and gas condition after the prism compressor assuming sech^2-shape. In the case of Ar pressure of 3 bar with incident energy of 226 μJ, a maximum broadening with foot-to-foot bandwidth of 60 nm, which corresponds to the FL duration of 350 fs, is obtained. However, the measured pulse duration is 480 fs.

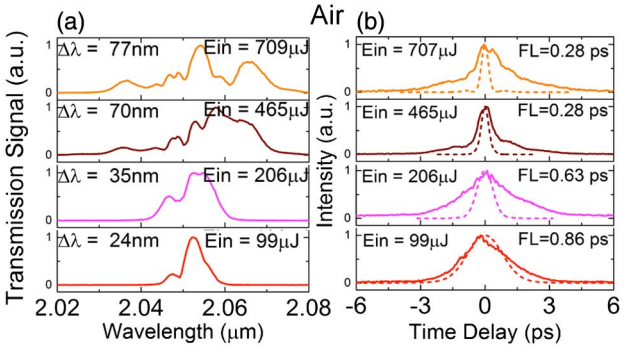

Fig. 3. (a) Spectral evolution of the 19-cell fiber output in the presence of ambient air for increasing input energy. (b) Corresponding measured autocorrelations (solid lines) along with their calculated FL autocorrelation (dotted lines).

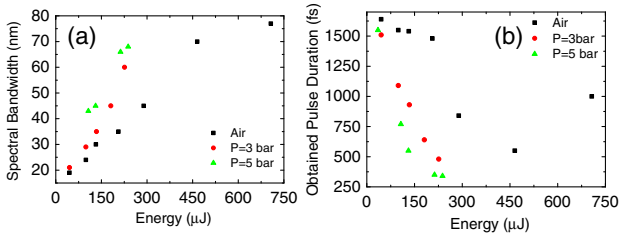

Fig. 4. (a) Spectral broadening with increasing incident energy in 19-cell fiber of 3.5 m length in the presence of air and Ar pressure of 3 and 5 bar; (b) shows their corresponding measured pulse duration.

Similarly, the experiments were also repeated with 5 bar of Ar up to incident energy of 238 μJ. The maximum bandwidth achieved in this case is 68 nm, leading to FL pulse duration of 280 fs and measured pulse duration of 350 fs. The increase in bandwidth with high pressure is due to higher nonlinearity present in the fiber. Thus at the energy level of ~240 μJ and 5 bar of Ar, the spectral broadening factor increased by a factor of ~2 with respect to air.

B. 7-Cell Kagome Fiber

To explore the effect of fiber core diameter on the nonlinear spectral broadening in these fibers, the previous experiments are repeated with 7-cell fiber (MFD = 44 μm) of length 3 m with slightly smaller core diameter and similar experimental conditions as those for the 19-cell fiber in the presence of air and Ar pressures of 3 and 5 bar. Figure 5(a) summarizes the broadening obtained at different incident energy in 7-cell fiber in the presence of air, and Ar pressure of 3 and 5 bar. Figure 5(b) summarizes the measured pulse duration after the prism compressor for the corresponding energy and gas conditions. It can be seen that, with this fiber in the case of air and incident energy of 238 μJ, maximum bandwidth of only 31 nm and measured pulse duration of 1.03 ps is obtained. However, in the case of Ar pressure of 3 and 5 bar, maximum broadening of 68 and 88 nm is obtained and the measured pulse duration is 450 and 280 fs, respectively. Thus, we see that the maximum broadening of 88 nm and shortest duration of 260 fs is achieved with 7-cell fiber and Ar pressure of 5 bar and incident energy of ~240 μJ. This is the shortest duration achieved in all the sets of experiments reported in this paper.

We also show the pulse evolution along the spectrum and time with increase in incident energy and Ar pressure of 5 bar. The spectrum is summarized in Fig. 6(a) and the measured autocorrelation along with FL duration is summarized in Fig. 6(b). It can be seen here that the compressed temporal profile obtained in the case of 5 bar of Ar in the 7-cell fiber with incident energy of 228 μJ exhibits

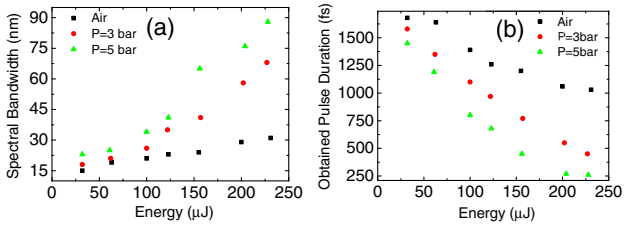

Fig. 5. (a) Spectral broadening with increasing incident energy in 7-cell fiber of 3 m length in the presence of air and Ar pressure of 3 and 5 bar; (b) shows their corresponding measured pulse duration.

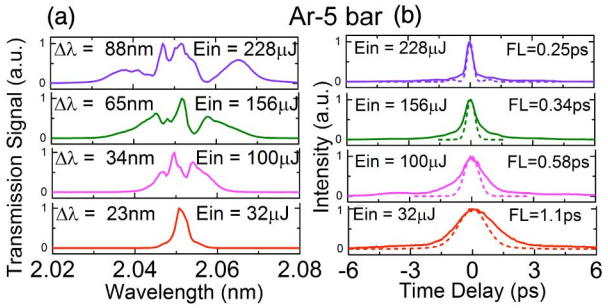

Fig. 6. (a) Spectrum evolution in 7-cell fiber of 3 m length for different incident pulse energies for Ar pressure of 5 bar; (b) shows their corresponding measured autocorrelation trace (solid lines) along with their calculated FL autocorrelation (dotted lines).

the least amount of energy going into the wings (top) and matches to that of Fourier-limited duration. With a transmission efficiency of 85% from the fiber and a compressor efficiency of 75%, the compressed energy obtained is 125 μJ. There is a ∼10% depolarization loss coming from the fiber, which explains the lower compression efficiency. By compensating for the depolarization, compression efficiency can be enhanced to 85%.

Finally, the output from the 7-cell fiber, with 5 bar of Ar and incident energy of 228 μJ, are characterized using a second-harmonic generation–frequency-resolved optical gating (SHG–FROG) setup employing a 200 μm thick BBO crystal. Figures 7(a) and 7(b) show the corresponding measured and reconstructed FROG traces with a reconstruction error of 1.4%. Figure 7(c) shows the retrieved (black) spectrum (∼40 nm FWHM) and its spectral phase (blue) together with the independently measured spectrum (red) that matches well. Finally, Fig. 7(d) shows the retrieved temporal intensity profile (solid black line) and the FL intensity profile (dotted red line) calculated from the independently measured spectrum. On the right-hand axis, the smooth and flat temporal phase profile is shown (blue curve), suggesting that only a small amount of chirp is remaining which can be compressed to 250 fs. However, the retrieved temporal profile still matches quite well with the calculated FL profile, with approximately 30% of the energy located in the wings.

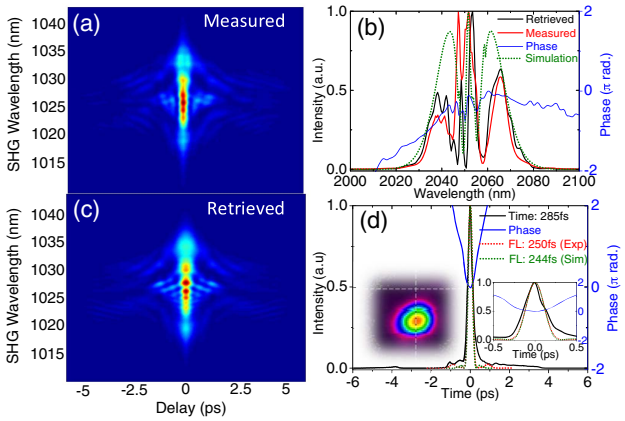

Fig. 7. SHG-FROG results of the pulses from 7-cell Kagome fiber filled with 5 bar of Ar: (a) Measured FROG trace. (b) Measured (red) and retrieved (black) spectrum with the spectral phase (blue). (c) Retrieved FROG trace. (d) Retrieved temporal intensity (black) and phase (blue) profiles.

To summarize the experiment: In the presence of air, spectral broadening of up to 77 and 31 nm are observed in 19-cell and 7-cell fibers at incident energies of 707 and 231 μJ with FL duration of 280 and 770 fs, respectively. For an Ar gas pressure of 3 bar, a broadening of up to 60 and 68 nm is obtained in 19-cell and 7-cell fiber, which corresponds to FL pulse durations of 350 and 320 fs, respectively, at an energy level of 227 μJ. Finally, for a 5 bar Ar, broadening of up to 68 and 88 nm was achieved, which corresponds to FL duration of 280 and 250 fs in 19-cell and 7-cell fiber, respectively. Using the prism compressor with a fixed apex separation optimized for the broadest spectrum of 88 nm, these pulses are compressed down to 300 and 285 fs for 19-cell and 7-cell fibers, respectively.

4. NUMERICAL MODELING

We theoretically model the propagation dynamics of the presented experiments in gas-filled Kagome fibers using a numerical model based on the one-dimensional nonlinear Schrödinger equation

$$i\frac{\partial A}{\partial z} = \frac{\beta_2}{2}\frac{\partial^2 A}{\partial t^2} - \gamma|A|^2 A, \tag{1}$$

where $\gamma = 5.9 \times 10^{-8}$/m. W is the nonlinear parameter, and $\beta_2 = -2345$ fs^2/m is the second-order dispersion of the gas-filled Kagome fiber including the geometric contribution of the 7-cell fiber, calculated for 1 bar of Ar pressure. Apart from self-phase modulation, in general, propagation of high-intensity pulses in a fiber may involve various nonlinear processes like plasma formation and higher-order Kerr effects. However, our experiments do not involve such high intensity and hence higher-order effects are sufficiently small to be ignored. In the model, a static pressure has been assumed throughout the length of the fiber.

The simulation results are calculated using the split-step Fourier technique. The input pulse we used is the transform-limited pulse computed from the experimentally measured spectrum and is propagated along a 7-cell fiber of length 3 m. Figure 8 shows the temporal and spectral evolution of this input pulse, with an energy of 135 μJ, along the 7-cell fiber filled with 1 bar Ar. The temporal profile does not change dramatically since the combined dispersion of the fiber and the gas is very low as the pulse propagates along the fiber, while its spectrum is significantly broadened. Since the dispersion is small, the output of the fiber is chirped, requiring external compression. The output spectrum overlays the FROG results shown in Fig. 7(b) (green), which are in good agreement with the measured spectrum. The FL pulse duration of the corresponding spectrum is 244 fs, also shown as an overlay in Fig. 7(d), which matches quite well to that of the FL pulse obtained from the measured spectrum.

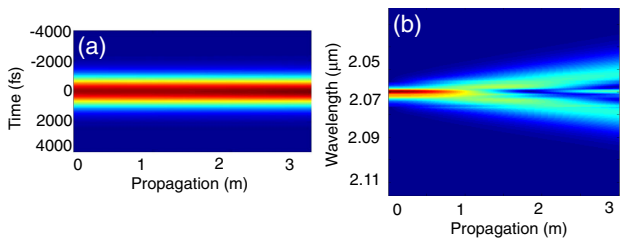

Fig. 8. Simulation results. (a) Temporal and (b) spectral evolution of the output pulse along the fiber length.

Some of the parameters used in the simulation are quite different from the ones in the experiment. For example, the pulse energy used in the fiber is 180 μJ; however, this excludes the coupling loss, which could not be independently determined. Furthermore, though a measurement of 5 bar was made near one end of the fiber, the exact pressure along the fiber length (as the gas flows through it) is not very realistic to determine. Such deviations can also arise due to deviation in the literature value of nonlinear refractive index of Ar gas used. Discrepancies of this nature are relatively standard for experiments such as this one [30], and the close agreement of the simulations with the experimental results lends credibility to these parameters.

5. SUMMARY AND OUTLOOK

In summary, we investigated both experimentally and numerically the nonlinear propagation dynamics of ps pulses in Kagome-type HC-PCF fibers in two different geometries, 7-cell and 19-cell designs. In the presence of air, maximum spectral broadening of 77 nm is observed in 19-cell fibers at incident energies of 707 μJ with FL duration of 280 fs. The experiments are also repeated in Ar-filled fibers at 3 and 5 bar pressure for both designs. Maximum broadening of 88 nm is achieved using 5 bar Ar in 7-cell fiber at incident energy of 227 μJ, which corresponds to FL duration of 250 fs in 7-cell fiber. Compression of these pulses is experimentally achieved down to 285 fs for 7-cell fibers. Hence, depending on the application, broadening in both 7-cell and 19-cell fiber can be useful. For experiments that need only a small amount of energy to be compressed as the one envisioned here, 7-cell fiber is optimum whereas, for experiments that require more compressed energy, 19-cell fiber is a better choice. The numerical results suggest that in the ps regime, the spectral broadening is mostly dominated by SPM and no higher-order effects are significant.

The 2 μm compressed output pulse from Kagome fiber enables generation of a stable supercontinuum in bulk solids in the MIR for seeding of OPAs. Since our front-end amplifier chain [38] delivers output pulses with 2.5 mJ energy, and only a small fraction of it is used for the Kagome compression stage, all the remaining energy from the amplifier can be used to pump OPA stages. The output of the amplifier chain is divided into two. One part, which has energy of 225 μJ, is used as the input for the Kagome nonlinear compression stage, while the remaining energy from the amplifier can be used to pump OPAs. Deriving the pump and seed pulses in the OPA from a common laser pulse permits generation of passively CEP-stable idler pulses [23]. Alternatively, the compressed pulse of 285 fs duration can be used as input in a second-stage Kagome fiber compressor. As the input pulse duration for this stage is much shorter and lies in the femtosecond range, its dispersion length reduces by 2–3 orders, thereby enabling pulse self-compression to few-cycle pulses. This work is an important step in the generation of sub-100 fs pulses and even few-to-single-cycle MIR pulses directly from a compact ps source.

Funding. European Research Council (ERC) (609920); Hamburg Centre for Ultrafast Imaging (CUI); Deutsche Forschungsgemeinschaft (DFG); Gordon and Betty Moore Foundation (ACHIP); Agence Nationale de la Recherche (ANR) (PHOTOSYNTH, ∑_LIM Labex Chaire); Région Limousin.

REFERENCES

1. H. Pires, M. Baudisch, D. Sanchez, M. Hemmer, and J. Biegert, "Ultrashort pulse generation in the mid-IR," Prog. Quantum Electron. **43**, 1–30 (2015).
2. C. I. Blaga, F. Catoire, P. Colosimo, G. G. Paulus, H. G. Muller, P. Agostini, and L. F. DiMauro, "Strong-field photoionization revisited," Nat. Phys. **5**, 335–338 (2009).
3. J. Dura, N. Camus, A. Thai, A. Britz, M. Hemmer, M. Baudisch, A. Senftleben, C. D. Schröter, J. Ullrich, R. Moshammer, and J. Biegert, "Ionization with low-frequency fields in the tunneling regime," Sci. Rep. **3**, 2675 (2013).
4. A. Ludwig, J. Maurer, B. W. Mayer, C. R. Phillips, L. Gallmann, and U. Keller, "Breakdown of the dipole approximation in strong-field ionization," Phys. Rev. Lett. **113**, 243001 (2014).
5. P. Colosimo, G. Doumy, C. I. Blaga, J. Wheeler, C. Hauri, F. Catoire, J. Tate, R. Chirla, A. M. March, G. G. Paulus, H. G. Muller, P. Agostini, and L. F. DiMauro, "Scaling strong-field interactions towards the classical limit," Nat. Phys. **4**, 386–389 (2008).
6. C. I. Blaga, J. Xu, A. D. DiChiara, E. Sistrunk, K. Zhang, P. Agostini, T. A. Miller, L. F. DiMauro, and C. D. Lin, "Imaging ultrafast molecular dynamics with laser-induced electron diffraction," Nature **483**, 194–197 (2012).
7. A. Chin, J. Bakker, and J. Kono, "Ultrafast electroabsorption at the transition between classical and quantum response," Phys. Rev. Lett. **85**, 3293–3296 (2000).
8. S. Ghimire, A. D. DiChiara, E. Sistrunk, U. B. Szafruga, P. Agostini, L. F. Dimauro, and D. A. Reis, "Redshift in the optical absorption of ZnO single crystals in the presence of an intense midinfrared laser field," Phys. Rev. Lett. **107**, 167407 (2011).
9. S. Ghimire, A. D. DiChiara, E. Sistrunk, P. Agostini, L. F. DiMauro, and D. A. Reis, "Observation of high-order harmonic generation in a bulk crystal," Nat. Phys. **7**, 138–141 (2011).
10. O. D. Mücke, "Isolated high-order harmonics pulse from two-color-driven Bloch oscillations in bulk semiconductors," Phys. Rev. B **84**, 081202(R) (2011).
11. D. Sanchez, M. Hemmer, M. Baudisch, S. L. Cousin, K. Zawilski, P. Schunemann, O. Chalus, C. Simon-Boisson, and J. Biegert, "7 μm, ultrafast, sub-millijoule-level mid-infrared optical parametric chirped pulse amplifier pumped at 2 μm," Optica **3**, 147–150 (2016).
12. F. Silva, D. R. Austin, A. Thai, M. Baudisch, M. Hemmer, D. Faccio, A. Couairon, and J. Biegert, "Multi-octave supercontinuum generation from mid-infrared filamentation in a bulk crystal," Nat. Commun. **3**, 807 (2012).
13. H. Liang, P. Krogen, R. Grynko, O. Novak, C. Chang, G. J. Stein, D. Weerawarne, B. Shim, F. X. Kärtner, and K. Hong, "Three-octave-spanning supercontinuum generation and of mid-infrared filaments in dielectrics," Opt. Lett. **40**, 1069–1072 (2015).
14. T. Popmintchev, M.-C. Chen, D. Popmintchev, P. Arpin, S. Brown, S. Alisauskas, G. Andriukaitis, T. Balciunas, O. D. Mücke, A. Pugzlys, A. Baltuska, B. Shim, S. E. Schrauth, A. Gaeta, C. Hernandez-Garcia, L. Plaja, A. Becker, A. Jaron-Becker, M. M. Murnane, and H. C. Kapteyn, "Bright coherent ultrahigh harmonics in the keV X-ray regime from mid-infrared femtosecond lasers," Science **336**, 1287–1291 (2012).
15. K. F. Mak, J. C. Travers, N. Y. Joly, A. Abdolvand, and P. St. J. Russell, "Two techniques for temporal pulse compression in gas-filled hollow-core Kagomé photonic crystal fiber," Opt. Lett. **38**, 3592–3595 (2013).
16. M. Hemmer, M. Baudisch, A. Thai, A. Couairon, and J. Biegert, "Self-compression to sub-3-cycle duration of mid-infrared optical pulses in dielectrics," Opt. Express **21**, 28095–28102 (2013).
17. O. Chalus, A. Thai, P. K. Bates, and J. Biegert, "Six-cycle mid-infrared source with 3.8," Opt. Lett. **35**, 3204 (2010).
18. V. Petrov, "Parametric down-conversion devices: the coverage of the mid-infrared spectral range by solid-state laser sources," Opt. Mater. **34**, 536–554 (2012).
19. P. Malevich, G. Andriukaitis, T. Flöry, A. J. Verhoef, A. Fernández, S. Ališauskas, A. Pugžlys, A. Baltuška, L. H. Tan, C. F. Chua, and P. B. Phua, "High energy and average power femtosecond laser for driving mid-infrared optical parametric amplifiers," Opt. Lett. **38**, 2746–2749 (2013).
20. C. R. Phillips, J. Jiang, C. Mohr, A. C. Lin, C. Langrock, M. Snure, D. Bliss, M. Zhu, I. Hartl, J. S. Harris, M. E. Fermann, and M. M. Fejer, "Widely tunable midinfrared difference frequency generation in

orientation-patterned GaAs pumped with a femtosecond Tm-fiber system," Opt. Lett. **37**, 2928–2930 (2012).
21. A. Dergachev, "High-energy, kHz-rate, picosecond, 2-μm laser pump source for mid-IR nonlinear optical devices," Proc. SPIE **8599**, 85990B (2013).
22. D. Brida, M. Marangoni, C. Manzoni, S. De Silvestri, and G. Cerullo, "Two-optical-cycle pulses in the mid-infrared from an optical parametric amplifier," Opt. Lett. **33**, 2901–2903 (2008).
23. G. Cerullo, A. Baltuška, O. D. Mücke, and C. Vozzi, "Few-optical-cycle light pulses with passive carrier-envelope phase stabilization," Laser Photonics. Rev. **5**, 323–351 (2011).
24. P. Malevich, T. Kanai, H. Hoogland, R. Holzwarth, A. Baltuška, and A. Pugžlys, "Broadband mid-infrared pulses from potassium titanyl arsenate/zinc germanium phosphate optical parametric amplifier pumped by Tm, Ho-fiber-seeded Ho:YAG chirped-pulse amplifier," Opt. Lett. **41**, 930–933 (2016).
25. F. Benabid and P. J. Roberts, "Linear and nonlinear optical properties of hollow core photonic crystal fiber," J. Mod. Opt. **58**, 87–124 (2011).
26. F. Benabid, "Hollow-core photonic bandgap fibre: new light guidance for new science and technology," Philos. Trans. R. Soc. A **364**, 3439–3462 (2006).
27. F. Couny, F. Benabid, P. J. Roberts, P. S. Light, and M. G. Raymer, "Generation and photonic guidance of multi-octave optical-frequency combs," Science **318**, 1118–1121 (2007).
28. Y. Y. Wang, N. V. Wheeler, F. Couny, P. J. Roberts, and F. Benabid, "Low loss broadband transmission in hypocycloid-core Kagome hollow-core photonic crystal fiber," Opt. Lett. **36**, 669–671 (2011).
29. Y. Y. Wang, X. Peng, M. Alharbi, C. F. Dutin, T. D. Bradley, F. Gérôme, M. Mielke, T. Booth, and F. Benabid, "Design and fabrication of hollow-core photonic crystal fibers for high-power ultrashort pulse transportation and pulse compression," Opt. Lett. **37**, 3111–3113 (2012).
30. B. Debord, M. Alharbi, L. Vincetti, A. Husakou, C. Fourcade-Dutin, C. Hoenninger, E. Mottay, F. Gérôme, and F. Benabid, "Multi-meter fiber-delivery and pulse self-compression of milli-joule femtosecond laser and fiber-aided laser-micromachining," Opt. Express **22**, 10735–10746 (2014).
31. J. Nold, P. Hölzer, N. Y. Joly, G. K. L. Wong, A. Nazarkin, A. Podlipensky, M. Scharrer, and P. St.J. Russell, "Pressure-controlled phase matching to third harmonic in Ar-filled hollow-core photonic crystal fiber," Opt. Lett. **35**, 2922–2924 (2010).
32. O. H. Heckl, C. R. E. Baer, C. Kränkel, S. V. Marchese, F. Schapper, M. Holler, T. Südmeyer, J. S. Robinson, J. W. G. Tisch, F. Couny, P. Light, F. Benabid, and U. Keller, "High harmonic generation in a gas-filled hollow-core photonic crystal fiber," Appl. Phys. B **97**, 369–373 (2009).
33. H. Ren, A. Nazarkin, J. Nold, and P. St.J. Russell, "Quasi-phase-matched high harmonic generation in hollow core photonic crystal fibers," Opt. Express **16**, 17052–17059 (2008).
34. J. M. Dudley, G. Genty, and S. Coen, "Supercontinuum generation in photonic crystal fiber," Rev. Mod. Phys. **78**, 1135–1184 (2006).
35. F. Emaury, C. J. Saraceno, B. Debord, D. Ghosh, A. Diebold, F. Gèrôme, T. Südmeyer, F. Benabid, and U. Keller, "Efficient spectral broadening in the 100-W average power regime using gas-filled Kagome HC-PCF and pulse compression," Opt. Lett. **39**, 6843–6846 (2014).
36. T. Balciunas, C. Fourcade-Dutin, G. Fan, T. Witting, A. A. Voronin, A. M. Zheltikov, F. Gerome, G. G. Paulus, A. Baltuska, and F. Benabid, "A strong-field driver in the single-cycle regime based on self-compression in a Kagome fibre," Nat. Commun. **6**, 6117 (2015).
37. O. H. Heckl, C. J. Saraceno, C. R. E. Baer, T. Südmeyer, Y. Y. Wang, Y. Cheng, F. Benabid, and U. Keller, "Temporal pulse compression in a xenon-filled Kagome-type hollow-core photonic crystal fiber at high average power," Opt. Express **19**, 19142–19149 (2011).
38. K. Murari, H. Cankaya, P. Kroetz, G. Cirmi, P. Li, A. Ruehl, I. Hartl, and F. X. Kärtner, "Intracavity gain shaping in millijoule-level, high gain Ho:YLF regenerative amplifiers," Opt. Lett. **41**, 1114–1117 (2016).
39. D. Wang, Y. Leng, and Z. Xu, "Measurement of nonlinear refractive index coefficient of inert gases with hollow-core fiber," Appl. Phys. B **111**, 447–452 (2013).